

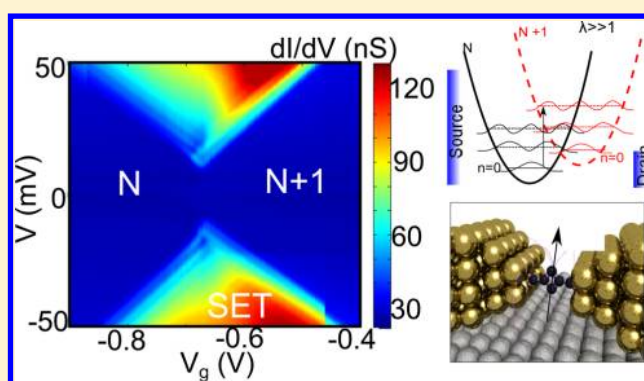
Franck–Condon Blockade in a Single-Molecule Transistor

Enrique Burzurí,^{*,†} Yoh Yamamoto,[‡] Michael Warnock,[‡] Xiaoliang Zhong,[‡] Kyungwha Park,^{‡,†} Andrea Cornia,[§] and Herre S. J. van der Zant[†][†]Kavli Institute of Nanoscience, Delft University of Technology, P.O. Box 5046, 2600 GA Delft, The Netherlands[‡]Department of Physics, Virginia Tech, Blacksburg, Virginia 24061, United States[§]Department of Chemical and Geological Sciences and INSTM, University of Modena and Reggio Emilia, via G. Campi 183, I-41125 Modena, Italy

Supporting Information

ABSTRACT: We investigate vibron-assisted electron transport in single-molecule transistors containing an individual Fe₄ Single-Molecule Magnet. We observe a strong suppression of the tunneling current at low bias in combination with vibron-assisted excitations. The observed features are explained by a strong electron–vibron coupling in the framework of the Franck–Condon model supported by density-functional theory.

KEYWORDS: Single-molecule magnets, molecular spintronics, Franck–Condon blockade, electron–vibron coupling



Vibrational modes (vibrons) play an essential role in the mechanics of a wide variety of nanostructures. In addition, they can couple to the electric charge, affecting the electrical transport through such nanoelectromechanical (NEMS) systems. Electron–vibron coupling has been experimentally observed, for instance, as vibron-assisted transport excitations in carbon nanotubes,^{1–4} in single molecules embedded in a solid-state transistor^{5–9} or probed by a scanning tunneling microscope (STM) configuration.^{10,11} When vibrational modes are mechanically excited in NEMS, they may induce mechanical instabilities.^{12–14} In magnetic molecules, the molecular vibrations may couple to spin degrees of freedom and play an important role in the molecular spin relaxation.¹⁵ Very recently, experimental evidence of such spin–vibron coupling was reported for a single-molecule magnet (SMM) TbPc₂ grafted onto a carbon nanotube.¹⁶ In that case, the reversal of the SMM magnetic moment via an external magnetic field was indirectly observed in the conductance map from the coupling to vibrational excitations of the nanotube. Therefore, electron–vibron coupling may be in principle used to detect the magnetic states of nanostructures and, conversely, to manipulate their transport and magnetic properties.

An interesting feature induced by electron–vibron coupling is the Franck–Condon (FC) blockade effect which occurs when electric charge is strongly coupled to vibrations. A manifestation of the FC blockade effect is that single-electron tunneling is suppressed at low bias for any gate voltage.^{17,18} It was first observed by Weig et al.¹⁹ in electron transport through GaAs/AlGaAs quantum dots of several hundreds of nanome-

ters. The FC blockade effect was later observed in suspended carbon nanotubes^{2,3} that are typically orders of magnitude larger than individual molecules. So far, however, the FC blockade effect has not been systematically analyzed in single-molecule junctions despite several experimental studies focusing on electron–vibron coupling.

In this Letter, we show experimental evidence of the FC blockade effect in electron transport via an individual magnetic molecule and present supporting calculations from density-functional theory (DFT). We investigate sequential electron tunneling (SET) through a SMM Fe₄²⁰ in a three-terminal configuration shown in Figure 1. We observe a dramatic suppression of current at low bias in combination with evenly spaced lines parallel to the Coulomb diamond edges in the conducting region. The suppression of current cannot be lifted by a gate voltage. The energy spacing of the excitations is 2.6 meV and is not affected by an applied magnetic field, thereby ruling out a possible magnetic origin. The energy spacing and the estimated resultant electron–vibron coupling constant are consistent with our DFT-calculated values. In addition, the DFT calculations suggest that the electron–vibron coupling can be enhanced by avoiding chemical bonding at the interface. Our findings clearly indicate strong electron–vibron coupling in magnetic molecules at the single-molecule level. They also

Received: February 10, 2014

Revised: April 24, 2014

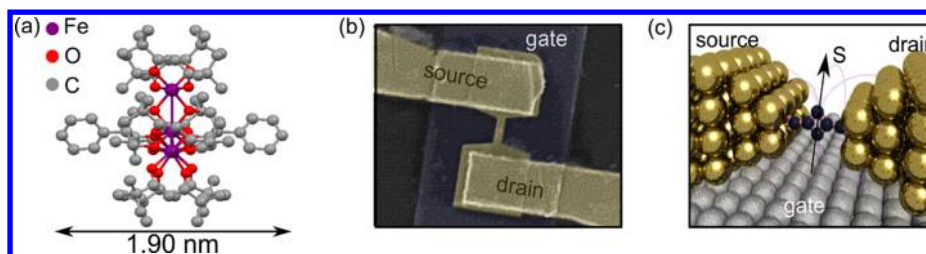


Figure 1. Fe_4 single-molecule transistor. (a) Sketch of the Fe_4 SMM. The magnetic core is made of 4 Fe^{3+} ions (purple) surrounded by an organic shell (gray and red). Hydrogen atoms are not shown for clarity. The size of the molecule from ring to ring is 1.90 nm. (b) SEM image and (c) sketch of a molecular three-terminal transistor. An individual molecule is linked to gold source and drain electrodes that electrically bias the molecule. An underlying gate electrode is used to tune the levels of the molecule independently from the bias voltage (gate oxide separating gate from source/drain electrodes not shown).

open a more general route to investigate new rich physics in single-molecule transistors containing individual magnetic molecules; examples include studies of the effects of intrinsic molecular vibrations on quantum interferences²¹ and on magnetic relaxation as a source of decoherence for SMM-based qubits.²²

The structure of the Fe_4 SMM²⁰ with formula $[\text{Fe}_4(\text{L})_2(\text{dpm})_6]$ is shown in Figure 1a. The Fe_4 molecule consists of four Fe^{3+} ions encapsulated in a hydrophobic shell made up of tert-butyl and phenyl groups from dpm^- and L3^- ligands, respectively. One Fe^{3+} ion at the center is antiferromagnetically coupled with three Fe^{3+} ions at the vertices of a triangle via oxygen bridges. The total spin in the ground state is $S = 5$ and a magnetic anisotropy barrier of 16 K must be overcome to reverse the magnetic moment. The size of the Fe_4 SMM is 1.90 nm along the direction defined by the phenyl rings.

A representative scanning electron microscope (SEM) image of the three-terminal device configuration is shown in Figure 1b. Electromigration is used to thin the Au wire and is followed by self-breaking in a solution of Fe_4 molecules to complete the device. Figure 1c schematically shows the sample layout: a single Fe_4 molecule is electrically linked to source and drain Au electrodes in order to apply a bias voltage to it. The Fe_4 molecule is not functionalized with specific surface-binding groups so that van der Waals interactions are responsible for the molecule–electrode coupling. An underlying gate electrode is used to tune the levels of the molecule independently from the bias voltage, as illustrated in Figure 1c. Importantly, our previous measurements showed that the magnetic structure of Fe_4 is preserved in a three-terminal configuration.²³ Measurements are performed at 1.8 K unless specified otherwise.

Figure 2a shows a differential conductance color map in which dI/dV is plotted as a function of bias V and gate voltage V_g . Low-conductance regions (left and right blue areas) are indicative of two different charge states N and $N + 1$ that are accessible using the gate voltage. In this Coulomb blockade regime, the charge is stabilized within the molecule. Note that only two charge states are available, indicative of high addition energies as expected for a SMM. Strong high-conductance resonances, indicating SET through the molecule, separate adjacent charge states. The coupling of the molecule to the electrodes (Γ_L, Γ_R) is of the order of 1 meV and is obtained from the full width at half-maximum (fwhm) of the Coulomb edges.

Interestingly, two remarkable features are observed in the dI/dV map. First, SET is highly suppressed at low bias below a threshold value $V_{\text{th}} = \pm 7.4$ meV. As a result, the Coulomb

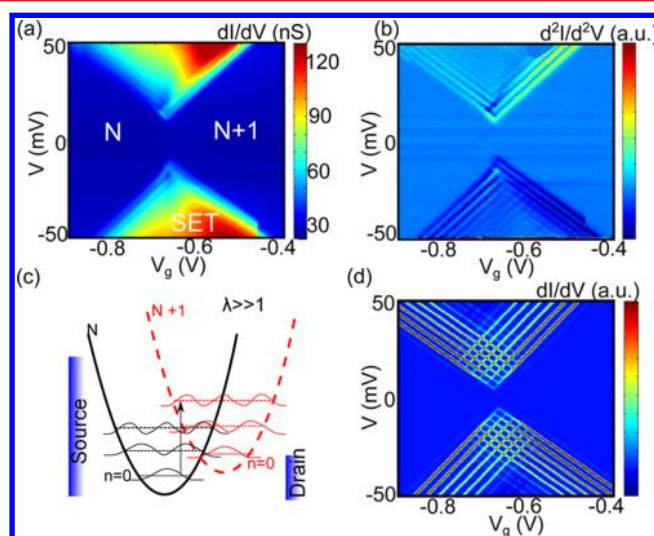


Figure 2. Franck–Coulomb blockade in a molecular junction containing a single Fe_4 molecule. (a) Differential conductance (dI/dV) color map measured in an Fe_4 molecular junction as a function of bias V and gate voltage V_g . Low-bias SET is suppressed below $V_{\text{th}} = 7.4$ meV and the Coulomb blockade cannot be lifted by V_g . Periodic excitations appear within the SET regime at positive and negative bias. The energy spacing between excitations is $\Delta E = 2.6$ meV. (b) Numerical derivative of the dI/dV color plot shown in (a). Periodic excitations running parallel to the Coulomb diamond edges become more visible. (c) Schematic representation of the Franck–Coulomb model for strong electron–vibron coupling λ . For high values of λ , the equilibrium coordinates in adjacent charge states are significantly shifted from each other. Then, vibronic ground-state to ground-state transitions become exponentially suppressed but ground-state to excited-states become available when V matches the energy of the excited vibrons ($n\hbar\omega$). (d) Calculated dI/dV color map by introducing the electron–vibron coupling in the rate equations.²⁵ The values of the temperature and the vibron energy used in the model are those obtained from the experiment ($T = 1.8$ K and $\Delta E \sim \hbar\omega_0 = 2.6$ meV). The best agreement is obtained for $\lambda = 2.21$.

diamond edges do not intersect at zero bias, that is, no dI/dV peak is observed at zero bias. This low-bias gap cannot be lifted by sweeping the gate voltage. Second, evenly spaced lines parallel to the Coulomb diamond edges are observed at positive and negative bias for $|V| > |V_{\text{th}}|$ (see Figure 2a). The lines become more visible when a numerical derivative of the dI/dV is taken as shown in Figure 2b. The energy spacing between these excitations is $\Delta E = 2.6$ meV. In the presence of a magnetic field, the Coulomb diamonds shift in gate as a result of the magnetic properties of the Fe_4 SMM. Interestingly, the value of ΔE is independent of applied magnetic field and

therefore we rule out a magnetic origin for the excitations (see Supporting Information for details). Moreover, the value of ΔE is symmetric with respect to the bias polarity and it is independent of the charge state, which is fingerprint of a vibronic origin. We emphasize that these two features with similar values of ΔE are observed for two additional junctions, each of which contains a single Fe_4 molecule. A discussion on the features of these additional junctions are presented in the Supporting Information. However, not all the Fe_4 molecular junctions show FC blockade as we discuss later.

The zero-bias conductance suppression may originate from the FC blockade effect^{17,24} that occurs when the dimensionless electron–vibron coupling λ is strong, that is, $\lambda \gg 1$. So far, direct experimental evidence of the effect has been reported for carbon nanotubes^{2,3} and semiconductor quantum dots,¹⁹ which are about 100 times larger in size than Fe_4 . Figure 2c illustrates the FC blockade model. For a system with a large value of λ , the equilibrium coordinates of the electronic ground state greatly differ from those of an electronic excited state. In the present case of Fe_4 , this corresponds to the case that the equilibrium geometry of the N charge state is very different from that of the $N + 1$ charge state, as sketched in Figure 2c. A transition from the vibrational ground level $n = 0$ of the N state to the vibrational ground level of the $N + 1$ state is exponentially suppressed with λ .¹⁷ The low-bias gap observed in Figure 2b is due to the suppression of this transition. However, the probability for transitions to occur from the $n = 0$ level of the N state to the $n \neq 0$ levels of the $N + 1$ state increases with a FC factor²⁴

$$\mathcal{F}_{n,0} = \frac{\lambda^{2n}}{n!} e^{-\lambda^2} \quad (1)$$

where n is a vibrational quantum number with frequency ω_0 , assuming that only one vibrational mode is considered. Note that the FC factor only depends on the dimensionless quantities λ and n .

Transitions involving higher-energy vibrational levels ($n \neq 0$) start to contribute to the sequential tunneling when $n > \lambda^2 / (2 \log \lambda) \sim \lambda^2$ (see also eq 1). The observed parallel lines in the SET region in Figure 2b are due to such transitions and therefore the energy spacing ΔE of the lines corresponds to $\hbar\omega_0$. The suppression of the conductance is predicted to be prominent for equilibrated vibrons with zero relaxation time¹⁷ and for $k_B T \ll \hbar\omega_0$, which meets our experimental conditions. The FC blockade is lifted when the bias voltage matches a multiple of vibrational energy, $n\hbar\omega_0$, at a threshold bias voltage V_{th} of about $\lambda^2 \hbar\omega_0$.¹⁷ Using the experimental values of $\hbar\omega_0$ and V_{th} , we extract the value $\lambda = 1.7$.

To corroborate our interpretation of the observed conductance map we simulate a dI/dV map using a minimal model Hamiltonian^{24,25} with $\hbar\omega_0 = 2.6$ meV obtained from the measurements. We consider up to $n = 10$ and solve the standard master equation to find the dI/dV map.²⁵ A good quantitative agreement is found for $\lambda = 2.21$. For simplicity, the Hamiltonian includes neither spin degrees of freedom of an electron nor the magnetic moment of the Fe_4 , which is justified because the parallel lines do not change with an applied magnetic field. The resulting dI/dV map, shown in Figure 2d, reproduces the main features of the measurements, such as the low-bias gap and the presence of equally spaced lines running parallel to the diamond edges.

The value of λ can be independently estimated from the dI/dV peaks ($(dI/dV)_{\text{max}}$) of the SET excitations as a function of V

at a given V_g .^{3,9} Figure 3a shows dI/dV versus V at a fixed $V_g = -0.711$ V. The background contribution due to direct

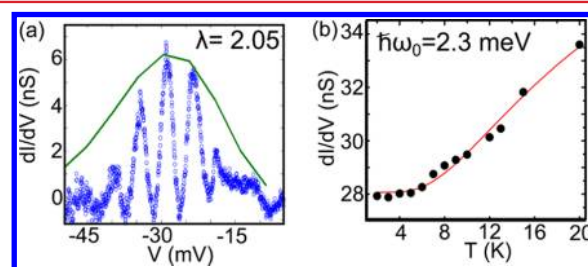


Figure 3. Analysis of the Franck–Cordon blockade. (a) Differential conductance measured as a function of V at $V_g = -0.711$ V. The background signal due to direct tunneling between the electrodes has been subtracted. The solid line is a fit to $(dI/dV)_{\text{max}}$ using the Franck–Cordon progression described in the main text. We obtain $\lambda = 2.05$, a value that is consistent with the λ estimated from the size of the low-bias gap and the value obtained with the rate equations. (b) Temperature dependence of $(dI/dV)_{\text{max}}$ measured at $V_g = -0.700$ V and $V = 12$ mV corresponding to the Coulomb blockade regime. From the fit (solid line) we obtain $\hbar\omega_0 = 2.3$ meV. This energy is consistent with the energy spacing of the excited vibronic states ($\Delta E = 2.6$ meV).

tunneling between the electrodes is subtracted from the data. The solid line in Figure 3a represents a fit of $(dI/dV)_{\text{max}}$ to the FC factor defined in eq 1 with $\lambda = 2.05$, which within the uncertainty is consistent with the value of λ estimated from the low-bias gap in Figure 2. Note that the curve does not fit the low-bias region because eq 1 does not take into account contributions from nonresonant cotunneling that are important in this region. The average λ obtained from different dI/dV traces is 2.0 ± 0.2 (see Supporting Information)

The value of ω_0 can also be independently estimated from the temperature dependence of dI/dV in the Coulomb blockade regime. Figure 3b shows dI/dV at different temperatures measured at $V_g = -0.700$ V and $V = 12$ mV, which corresponds to the Coulomb blockade regime close to the diamond edge at positive bias. Note that $V = 12$ mV is greater than the threshold bias to lift the Franck–Cordon blockade. The value of dI/dV increases nonlinearly with increasing temperature. Such an increase of the conductance with the temperature can be explained with the absorption by the tunneling electrons of one or more vibrational quanta of the molecule³ (see Figure S5 in the Supporting Information). Previously forbidden transitions become available and sidebands of sequential tunneling may appear in the Coulomb blockade regime parallel to the Coulomb diamond edges.^{1,3,18,26} It is observed in carbon nanotubes³ that the intensity of the absorption sidebands increases with increasing T . If the enhanced tunneling in the Coulomb blockade regime is indeed due to the absorption of vibrons, the temperature dependence obeys Bose–Einstein statistics so that $(dI/dV)_{\text{max}} \propto 1/k_B T \times 1/(\exp(\hbar\omega_0/k_B T) - 1)$.³ The solid line in Figure 3b is a fit to the experimental data with $\hbar\omega_0 = 2.3$ meV, which is consistent with the energy spacing of the excitations $\Delta E = 2.6$ meV. Note that the dI/dV maps measured at 1.8 K do not show evidence of absorption-induced sidebands, indicating a fast vibrational relaxation of the vibrational mode²⁶ in combination with a low T compared with the energy of the vibron ($k_B T \ll \hbar\omega_0$). Only by increasing temperature we start to observe signatures of peaks within the Coulomb blockade region

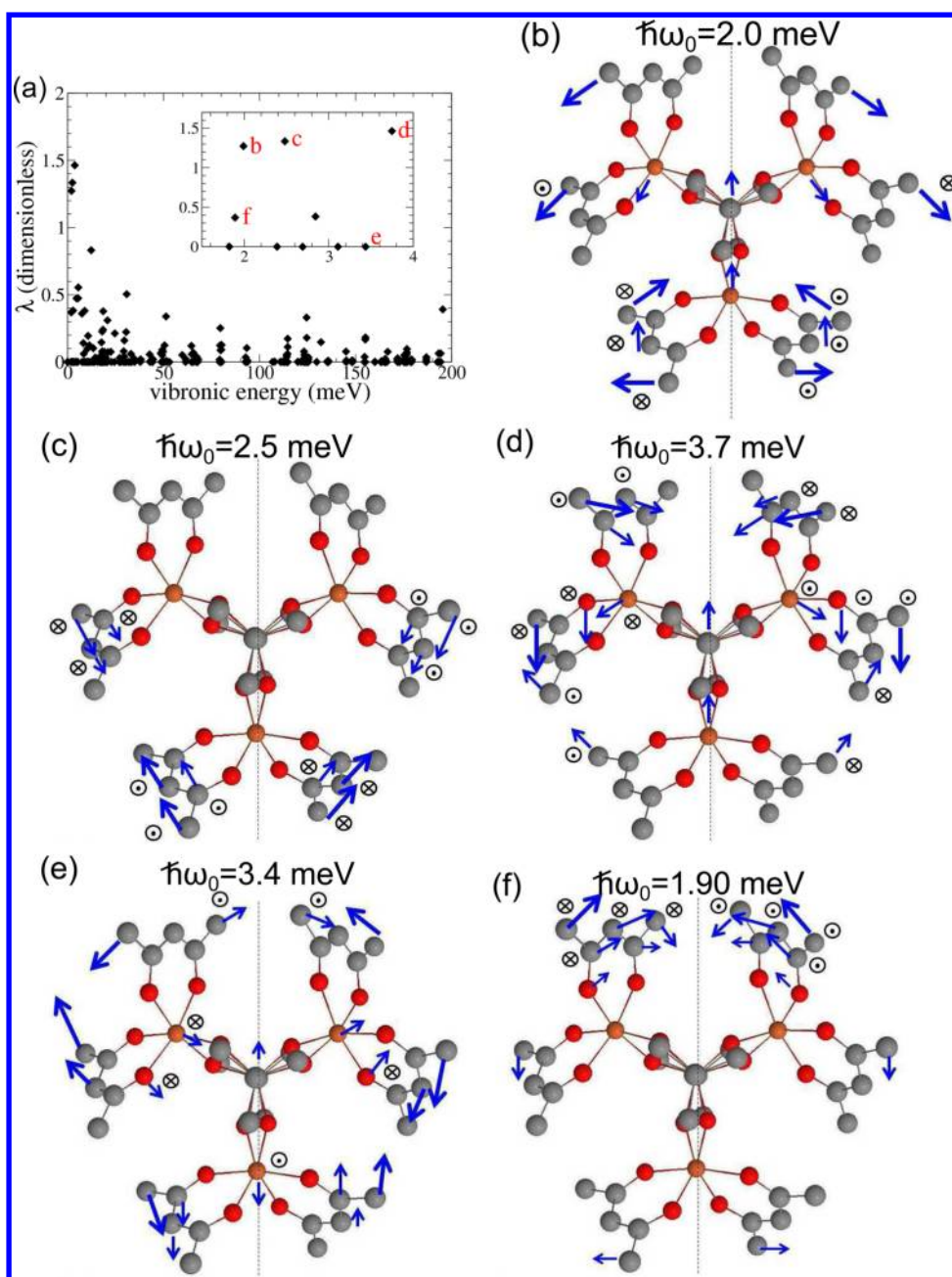


Figure 4. DFT results for Fe_4 SMM. (a) Calculated electron–vibron coupling constant versus $\hbar\omega$ for Fe_4 . The inset is a zoom-in of λ versus $\hbar\omega$ for Fe_4 showing the five normal modes illustrated in (b–f): $\hbar\omega = 2.0, 2.5, 3.7, 3.4,$ and 1.9 meV, respectively. The Fe_4 molecules in (b–f) are projected onto the x – y plane with the dashed vertical lines indicating the y -axis. The color code in (b–f) is Fe (orange), O (red), and C (gray). H atoms and phenyl rings are not shown. The length of the arrows represents the magnitude of the displacements. The circled dot and circled cross are displacements along the positive and negative z -axes. Only significant displacements are shown.

because vibrons can be excited and their relaxation time becomes longer (see Supporting Information).

In this work, we do not include the effect of oscillations of the center of motion of the Fe_4 relative to the electrodes, although the frequency could be of the order of millielectronvolts, as shown for the C_{60} molecule.⁵ The oscillations are coupled to the Fe_4 via displacement-dependent tunneling matrix elements.²⁷ We estimate that the coupling strength of the oscillations can not induce Franck–Condon blockade. More details on this issue can be found in the Supporting Information

So far, the analysis of our experimental data consistently shows that the measured conductance map is due to the FC

blockade effect with $\hbar\omega_0 = 2.6$ meV and $\lambda \simeq 2.2$. Henceforth, we present results obtained from DFT calculations on the Fe_4 molecule and compare them with the experimental values. We first find the optimized geometries for the neutral Fe_4 and singly charged Fe_4 molecules using DFT. Then, we calculate the normal modes of the neutral Fe_4 molecule within the simple harmonic oscillator approximation. In our calculations, we consider only an isolated Fe_4 molecule without Au electrodes. This is justified because the Fe_4 molecule is not covalently bonded to the electrodes. For each normal mode, we compute the dimensionless coupling constant²⁵ from

$$\lambda = \sqrt{\frac{\omega}{2\hbar}} \Omega^T M (\mathbf{R}_0 - \mathbf{R}'_0) \quad (2)$$

where ω and M are the normal-mode frequency and the square diagonal matrix of atomic masses, respectively. Ω^T is the transpose of the mass-weighted normal-mode column eigenvector with $\Omega^T M \Omega = 1$. Here, \mathbf{R}_0 and \mathbf{R}'_0 are column vectors corresponding to the optimized coordinates of the neutral and charged Fe_4 molecules, respectively.

Our DFT calculations show that only three vibrational modes with energies 2.0, 2.5, and 3.7 meV have a value of λ greater than unity such as 1.27, 1.33 and 1.46, respectively, as shown in the inset of Figure 4a. The rest of the vibrational modes have a value of λ much lower than unity except for several tens of modes with λ of the order of 0.1, as shown in Figure 4a. The three vibrational modes have energies close to the experimentally extracted energy values, and the coupling constants are similar to the experimental values. Despite having three normal modes with $\lambda > 1$, our transport calculations show only one broad dI/dV peak at the corresponding multiples of the vibrational excitation. This is due to the thermal broadening at 1.8 K (see Figure S6 in Supporting Information).

We now analyze the characteristics of the vibrational modes in order to understand why only a few of them have a strong coupling constant. The three modes with strong coupling are shown in Figure 4b–d, where the dashed vertical lines represent the y -axis. The Fe_4 molecule of interest has 2-fold (C_2) symmetry about this axis. Movies of the three modes are available in the Supporting Information. According to the group theory,²⁸ all the normal modes of the C_2 symmetric Fe_4 molecule can be classified into symmetric and antisymmetric modes about the y -axis, or A and B representations, respectively. One-half of the nonzero-frequency normal modes belong to the A representation and the other half to the B representation. We find that all the modes in the B representation have a very small value of λ , which is less than 0.00045 in our numerical accuracy, and that the value of λ for the modes in the A representation varies. For example, the normal mode shown in Figure 4e belongs to the B representation, and it has an electron–vibron coupling constant of 0.0001. There are several distinctive features in the three modes with strong coupling compared to other modes with weaker coupling: (i) The normal modes in Figure 4b–d belong to the A representation, (ii) the major vibrations are from heavier elements such as Fe, O, and C atoms, and (iii) the modes have low frequencies.

These observations concerning the strength of the electron–vibron coupling can be rationalized as follows. The coupling λ in eq 2 is proportional to the inner product between the normal-mode eigenvectors and the difference vector in the equilibrium coordinates of the neutral and charged Fe_4 molecules. Considering the 2-fold symmetry of an isolated Fe_4 molecule, it is likely that this symmetry can be preserved even for an Fe_4 molecule bridged between electrodes, because the molecule is not chemically bonded to them. If the charged Fe_4 molecule has the same 2-fold symmetry, then the coordinate difference vector also bears the 2-fold symmetry. This implies that for normal modes in the A representation, each term in eq 2 contributes to the coupling with the same sign so that the coupling constant can become large. However, when normal modes are in the B representation, terms in eq 2 cancel out, and the coupling constant becomes very small (i.e., $\lambda \ll 1$). See Figure 4e for an example. Note that this result

suggests that a Fe_4 molecule chemically bonded to electrodes may not bring strong electron–vibron coupling due to possible broken molecular symmetry. Furthermore, among the normal modes with the 2-fold symmetry, the coupling is expected to be stronger when the vibrations mainly arise from heavier elements such as Fe, O, and C atoms, rather than H atoms. This is due to the atomic mass term included in eq 2.

Finally, we discuss possible sources of discrepancy between the experimental data and the DFT calculations. The first source is that the distribution of an extra electron added (or tunneled) to a neutral Fe_4 molecule has not been experimentally determined. The DFT-calculated value of λ depends on the difference in equilibrium coordinates of the neutral and charged Fe_4 SMMs, as shown in eq 2. Changes in the distribution of the extra electron can significantly change this difference and they may break the molecular 2-fold symmetry. In our DFT calculations, we consider one particular charge distribution where the extra electron is uniformly distributed over all the four Fe ions. In the case of carbon nanotubes, it was reported that strong electron–vibron coupling is induced when the tunneled electron is localized.² The second source is that the value of λ depends on environmental factors,^{7,29} yet DFT calculations do not fully capture them, such as image charge effects, localized charge impurities, and various molecular orientations relative to the electrodes. In this direction, note that we do not observe FC blockade in all Fe_4 devices. Similarly, a variation of λ for different devices has also been observed for carbon nanotubes²⁹ and C_{140} molecules.⁷ The aforementioned two sources are correlated and make it difficult to theoretically precisely assign a particular mode as the cause of the FC blockade. A further study along this direction is interesting but beyond the scope of the current work.

In conclusion, we have studied single-electron transport via an individual Fe_4 SMM in three-terminal devices. We have observed a suppression of the low-bias conductance and explained its origin with a FC blockade effect caused by strong coupling between the electric charge and a vibrational mode of the Fe_4 . From a detailed comparison with the FC model, we extracted the values of the vibron frequency and electron–vibron coupling constant from our experimental data. The values agree with the DFT-calculated results, which also suggest the possibility of increasing the coupling by avoiding chemical bonding at the interface. This is the first direct experimental evidence of the FC blockade effect for a small magnetic molecule with a diameter of about 2 nm. Our findings will stimulate further research on the role of molecular vibrations in molecular transport and more specifically on the impact of such strong electron–vibron coupling on the molecular spin degrees of freedom.

■ ASSOCIATED CONTENT

📄 Supporting Information

Further details about the Fe_4 SMM, magnetic- and temperature-dependent measurements together with some statistics and details of the DFT calculations. This material is available free of charge via the Internet at <http://pubs.acs.org>.

■ AUTHOR INFORMATION

Corresponding Author

*E-mail: e.burzurilinares@tudelft.nl.

Notes

The authors declare no competing financial interest.

■ ACKNOWLEDGMENTS

The authors thank J. Seldenthuis, A. Zyazin, and J. M. Thyssen for discussions. This work was supported by the EU FP7 program under the Grant Agreement ELFOS, the project 618082 ACMOL, and the advanced ERC Grant (Mols@Mols). It was also supported by the Dutch funding organization NWO (VENI) and OCW. Y.Y., M.W., X.Z., and K.P. were supported by U.S. National Science Foundation DMR-0804665 and DMR-1206354 SDSC Trestles under DMR060009N and VT-ARC.

■ REFERENCES

- (1) LeRoy, B. J.; Lemay, S. G.; Kong, J.; Dekker, C. *Nature* **2004**, *432*, 371–374.
- (2) Sapmaz, S.; Jaillo-Herrero, P.; Blanter, Ya. M.; Dekker, C.; van der Zant, H. S. J. *Phys. Rev. Lett.* **2006**, *96*, 026801.
- (3) Leturcq, R.; Stampfer, C.; Inderbitzin, K.; Durrer, L.; Hierold, C.; Mariani, E.; Schultz, M. G.; von Oppen, F.; Ensslin, K. *Nat. Phys.* **2009**, *5*, 327–331.
- (4) Hüttel, A. K.; Witkamp, B.; Leijnse, M.; Wegewijs, M. R.; van der Zant, H. S. J. *Phys. Rev. Lett.* **2009**, *102*, 225501.
- (5) Park, H.; Park, J.; Lim, A. K. L.; Anderson, E. H.; Alivisatos, A. P.; McEuen, P. L. *Nature* **2000**, *407*, 57–60.
- (6) Park, J.; Pasupathy, A. N.; Goldsmith, J. I.; Chang, C.; Yaish, Y.; Petta, J. R.; Rinkoski, M.; Sethna, J. P.; Abruja, H. D.; McEuen, P. L.; Ralph, D. C. *Nature* **2002**, *417*, 722–725.
- (7) Pasupathy, A. N.; Park, J.; Chang, C.; Soldatov, A. V.; Lebedkin, S.; Bialczak, R. C.; Grose, J. E.; Donev, L. A. K.; Sethna, J. P.; Ralph, D. C.; McEuen, P. L. *Nano Lett.* **2005**, *5*, 203–207.
- (8) de Leon, N. P.; Liang, W.; Gu, Q.; Park, H. *Nano Lett.* **2008**, *8*, 2963–2967.
- (9) Osorio, E. A.; Ruben, M.; Seldenthuis, J. S.; Lehn, J.-M.; van der Zant, H. S. J. *Small* **2010**, *6*, 174–178.
- (10) Stipe, B. C.; Rezaei, M. A.; Ho, W. *Science* **1998**, *280*, 1732–1735.
- (11) Pradhan, N. A.; Lui, N.; Ho, W. *J. Phys. Chem. B* **2005**, *109*, 8513–8518.
- (12) Pistolesi, F.; Labarthe, S. *Phys. Rev. B* **2007**, *76*, 165317.
- (13) Weick, G.; Pistolesi, F.; Mariani, E.; von Oppen, F. *Phys. Rev. B* **2010**, *81*, 121409.
- (14) Weick, G.; von Oppen, F.; Pistolesi, F. *Phys. Rev. B* **2011**, *83*, 035420.
- (15) Gatteschi, D.; Sessoli, R.; Villain, J. *Molecular Nanomagnets*; Oxford University Press: New York, 2006.
- (16) Ganzhorn, M.; Klyatskaya, S.; Ruben, M.; Wernsdorfer, W. *Nat. Nanotechnol.* **2013**, *8*, 165–169.
- (17) Koch, J.; von Oppen, F. *Phys. Rev. Lett.* **2005**, *94*, 206804.
- (18) Koch, J.; Raikh, M. E.; von Oppen, F. *Phys. Rev. Lett.* **2006**, *96*, 056803.
- (19) Weig, E. M.; Blick, R. H.; Brandes, T.; Kirschbaum, J.; Wegscheider, W.; Bichler, M.; Kotthaus, J. P. *Phys. Rev. Lett.* **2004**, *92*, 046804.
- (20) Accorsi, S.; Barra, A.-L.; Caneschi, A.; Chastanet, G.; Cornia, A.; Fabretti, A. C.; Gatteschi, D.; Mortaló, C.; Olivieri, E.; Parenti, F.; Rosa, P.; Sessoli, R.; Sorace, L.; Wernsdorfer, W.; Zobbi, L. *J. Am. Chem. Soc.* **2006**, *128*, 4742–4755.
- (21) Zhong, X.; Cao, J. C. *J. Phys.: Condens. Matter* **2009**, *21*, 295602.
- (22) Stamp, P. C. E.; Gaita-Ariño, A. *J. Mater. Chem.* **2009**, *19*, 1718–1730.
- (23) Burzuri, E.; Zyazin, A. S.; Cornia, A.; van der Zant, H. S. J. *Phys. Rev. Lett.* **2012**, *109*, 147203.
- (24) Koch, J.; von Oppen, F.; Andreev, A. V. *Phys. Rev. B* **2006**, *74*, 205438.
- (25) Seldenthuis, J. S.; van der Zant, H. S. J.; Ratner, M. A.; Thijsen, J. M. *ACS Nano* **2008**, *2*, 1445–1451.
- (26) Lüffe, M. C.; Koch, J.; von Oppen, F. *Phys. Rev. B* **2008**, *77*, 125306.
- (27) Koch, J.; von Oppen, F.; Oreg, Y.; Sela, E. *Phys. Rev. B* **2004**, *70*, 195107.
- (28) Dresselhaus, M. S.; Dresselhaus, G.; Jorio, A. *Group Theory: Application to the Physics of Condensed Matter*; Springer-Verlag: Berlin 2008.
- (29) Osorio, E. A.; O'Neill, K.; Stuhr-Hansen, N.; Nielsen, O. F.; Bjørnholm, T.; van der Zant, H. S. J. *Adv. Mater.* **2007**, *19*, 281–285.